Computer Modeling in Engineering & Sciences
DOI:10.32604/cmes.2020.09842
Article

Novel Micromixer with Complex 3D-Shape Inner Units: Design, Simulation and Additive Manufacturing

Di Wang[1], Guangzhao Ye[1], Jingming Mai[2], Xiaomin Chen[1], Yongqiang Yang[1,*], Yang Li[1,*], Xiaojun Chen[1] and Jie Chen[1]

[1]School of Mechanical and Automotive Engineering, South China University of Technology, Guangzhou, 510640, China
[2]Department of Electrical Engineering and Information Technology, Karlsruhe Institute of Technology, Karlsruhe, 76131, Germany
*Corresponding Authors: Yongqiang Yang. Email: meyqyang@scut.edu.cn; Yang Li. Email: meyangli@scut.edu.cn
Received: 30 January 2020; Accepted: 30 March 2020

Abstract: In this paper, a novel micromixer with complex 3D-shape inner units was put forward and fabricated by metal Additive Manufacturing (AM). The design of the micromixer combined the constraints of selective laser melting technology and the factors to improve mixing efficiency. Villermaux-Dushman reaction system and Compute Fluid Design (CFD) simulation were conducted to investigate the performance and the mechanism of this novel micromixer to improve mixing efficiency. The research found that the best mixing efficiency of this novel micromixer could be gained when the inner units divided fluid into five pieces with a uniform volume. Compared with a conventional micromixer without obstacle in the channel, the micromixer designed in this research achieved higher mixing efficiency and reduce the pressure drop by 10.34%. The mixing behaviour in this novel micromixer was discussed, which mainly contains two types: collisions and swirls. Via collisions, the fluid micro masses would hit each other directly, which broke the boundaries of micro masses and promoted the interchange of species in the whole flow field. In swirls, the fluid micro masses were drawn into thin and long slices, which increased the size of the contact area and enhanced molecule diffusion. Finally, the application scheme of this novel micromixer was briefly discussed.

Keywords: Additive manufacturing (AM); micromixer; computational fluid dynamics (CFD); selective laser melting (SLM)

1 Introduction

The mixing process has a great influence on the quality of products in the chemical industry [1,2]. For example, processes like polymerization, crystallization, and precipitation are very sensitive to the mixing process [3,4]. Micromixer is a kind of continuous flow chemical synthesis device with a feature dimension from micron to millimeter that may have a considerable potential to improve the mixing process of the chemical reaction [5]. Due to the small size of the reacting channel, the ratio of surface-to-volume is large, which can bring a high capacity of mass transfer and heat transfer, so that the reactants inside can mix effectively and be cooled or heated quickly [6].

This work is licensed under a Creative Commons Attribution 4.0 International License, which permits unrestricted use, distribution, and reproduction in any medium, provided the original work is properly cited.

Since the invention of micromixer, it has become increasing valuable applications in the chemical industry [7], especially the fine chemical industry such as pharmaceutical production [8], nanostructured materials [9], and advanced molecular materials [10]. However, due to the small channel dimension, the flow regime is often laminar inside the micromixer, which makes the mixing process depend on the slow molecular diffusion. That limits the dimension of micromixers from tens to hundreds of microns to obtain good mixing efficiency. However, the small dimension of the channel decreases the productivity of chemical production and increases the cost of equipment and energy to meet the high demand for input power. The enlargement of the channel increases productivity and low down these costs but also reduce the mixing efficiency, which may lead to poor product quality [11,12]. These factors restrict the development of micromixer in industry.

Researchers have studied the relationship between the geometry and flow regime. The method combined CFD simulation with chemical experiment has been widely used to improve the performance of micromixer. Engler et al. [13] have studied the relationship between flow regime and mixing efficiency by CFD simulation and the Fourth-Bourne reaction system. They also proposed the T-mixer as one of the optimization probabilities which has a throttle and multiple groups of inlets. Bettermann et al. [14] developed a digital and lean development method for 3D-printed reactors based on the combination of CAD modeling and CFD simulation. Lu et al. [15] have researched the relationship between the dimensions of an asymmetrical T-type mixer and the mixing efficiency by CFD simulation and the Villermaux-Dushman reaction system. They discussed the scale-up strategy of mixing configuration as well.

In the manufacturing process, the micromixers are often fabricated by polydimethylsiloxane (PDMS) replica molding method. For example, Ansari et al. [16] used PDMS replica molding method to fabricate a novel micromixer replacing the mixing zone of a symmetrical T-type mixer with a group of rings, which can make splits and collisions of the fluid stream and improve the mixing efficiency. Some other methods, such as milling, the Lithographie, Galvanoformung and Abformung process (LIGA), electrical-discharge machining (EDM), etc., are applied as well [5]. However, these methods can only fabricate a micromixer with 2D-shape channel, which limits the optimization space.

Additive Manufacture (AM) is a rapidly developing technology in manufacturing. This technology breaks through the conventional thinking of deforming and removing the materials in the conventional manufacturing process and can realize a new manufacturing concept called “Net Shape Forming” which conforms to the new tide of “Green Manufacture” [17,18]. The biggest advantage of AM is that it forms a part by adding materials so that it does not need to consider how to remove the material to form the internal structure. This characteristic of AM is very suitable to fabricate a micromixer with the complex 3D-shape channel. Okafor et al. [19] fabricated a miniaturized continuous flow oscillatory baffled reactor with the Stereolithography (SLA) technology which is one of the AM processes. The results of the silver nanoparticle evaluation system showed that this micromixer could obtain satisfactory solution intersolubility results, which indicated a very high mixing efficiency. Guo et al. [20] designed a three-dimensional (3D) serpentine microchannel reactor and applied it in the biohydration of acrylonitrile, which indicated that the 3D reactor can help the fast reactions that are limited by mass transfer resistance. This case reflects the potential of AM in the field of micromixer manufacture.

In this study, metal material and selective laser melting (SLM) technology were applied to fabricate the micromixer, since metal materials perform high thermal conductivity and SLM is a mature AM technology in metal additive manufacturing [21]. A new micromixer with complex 3D-shape channel was designed and fabricated by SLM, considering both the constrain of SLM and the factors to improve mixing efficiency. Then the optimal feature size was investigated both by CFD simulation and the results of chemical experiments. The chemical experiments for evaluation were conducted with the Villermaux-Dushman parallel competitive reaction system. Based on the solution of CFD simulation, the flow field was

observed, and the advantages over the conventional micromixer were analyzed. In the end, the application scheme was briefly discussed.

2 Experimental Methods

2.1 Design of the Novel Micromixer

As shown in Fig. 1a, the internal channel structure of the micromixer is composed of axially arrayed unit bodies. The inner unit of the micromixer designed in this research is composed of two pairs of obstacles which are orthogonal quadrilateral pyramid tables, shown as Fig. 1b.

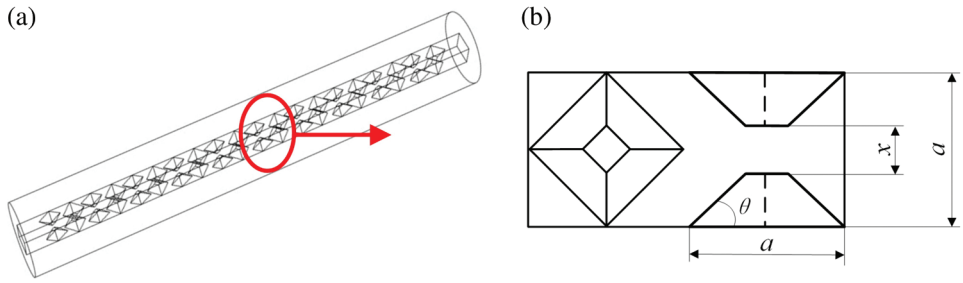

Figure 1: The sketches of the micromixer: (a) the sketch of the whole micromixer, (b) the dimension of the micromixer

The idea is that when a piece of fluid passes through the unit, it is split into a few pieces by the front edges and the gaps of the obstacles. These pieces of fluid flow forward along the inclines. They then converge in front of the next pair of obstacles which are orthogonal to the previous one. When the separated fluids converge, the convergent fluids collide and form swirls at the back of the obstacles due to their opposite component velocity. The collision of the fluids and the formation of the swirls disturb the flow, break the original laminar flow regime and strengthen convective diffusion, which directly pulls the components together, and shortens the diffusion distance of the components in the fluid. This process eventually improves the mixing efficiency of the micromixer.

As shown in Fig. 1b, the feature cross-section of the unit is determined by the side length of the channel a, the intersection angle between the edge and the wall θ, and the gap width between the obstacles x. Due to its irregular shape, the hydraulic diameter d which is used in the Eq. (1) of hydromechanics and regarded as the feature size is given as follow:

$$d = \frac{4A}{C} = \frac{2ax\sin\theta + (a-x)^2\cos\theta}{2a\sin\theta + (a-x)(1-\cos\theta)} \tag{1}$$

In Eq. (1), A means the area of the cross-section, and C means the circumference. Considering the accuracy of the SLM equipment used and the common size of micromixer, a was set to 2 mm. Moreover, θ was set to 45° which is a safe degree to form overhangs without support. Therefore, the Eq. (1) can be rewritten as follow:

$$d = \frac{x^2 + 4}{\left(1-\sqrt{2}\right)x + 2 \times \left(1+\sqrt{2}\right)} \tag{2}$$

In order to investigate the effect of x on mixing efficiency, a series of values were set to x: 0.2 mm, 0.4 mm, 0.6 mm, 0.8 mm, 1.0 mm, corresponding to the hydraulic diameter of 0.85 mm, 0.89 mm, 0.95 mm, 1.03 mm, 1.13 mm respectively according to the Eq. (2). The final models were 44 mm long with ten inner units and two 2 mm-long transition zones.

2.2 The Metal Material and SLM Equipment

The fluid impact, high pressure and the heat exchange inside the micromixer, result in a stronger corrosive environment. The Inconel 718 alloy powder with better corrosion resistance and an average particle size of 33.44 μm is chosen. The composition of the powder was shown as Tab. 1.

The SLM equipment used in this research was Dimetal-100 produced by Laseradd Technology (Guangzhou) Co., Ltd. The parameters to fabricate the micromixer were shown as Tab. 2.

Table 1: Chemical composition of the Inconel 718 alloy powder

Element	Ni	Cr	Fe	Nb	Mo	Ti	Al	Cu
Wt. %	52.91	19.20	17.32	5.16	3.17	0.65	0.54	0.13

Table 2: The parameters for manufacturing Inconel 718 alloy part

Item	Scanning strategy	Spiral angle	Laser power	Scanning speed	Scanning space	Layer thickness
Parameters	Spiral divisional strategy	30°	200 W	1000 mm/s	0.08 mm	0.03 mm

2.3 The Chemical Experiment for Evaluation

In the chemical experiment, the Villermaux-Dushman parallel competing reaction system was used. In this method, the concentration of I_3^- in the solution gained is considered as a probe to evaluate the mixing efficiency of the micromixer [22].

The chemical reactions occurred are as follows:

$$H^+ + H_2BO_3^- \rightarrow H_3BO_3 \quad \text{(i)}$$

$$5I^- + 6H^+ + IO_3^- \rightarrow 3I_2 + 3H_2O \quad \text{(ii)}$$

$$I^- + I_2 \leftrightarrow I_3^- \quad \text{(iii)}$$

Due to the characteristics of reaction (i) and (ii), reaction (i) always takes place ahead of reaction (ii). Reaction (ii) will occur only when there is an excess of H^+, and therefore reaction (iii) occur. However, the H^+ content is insufficient compared with $H_2BO_3^-$, which indicates a lack of H^+ in the channel. Therefore, reaction (ii) and (iii) can happen only when a local excess of H^+ appears, and the local excess of H^+ shows a heterogeneous mixing in the micromixer. For this reason, the concentration of the product of reaction (iii), i.e., I_3^-, can characterize the mixing performance of micromixer [23,24].

To characterize the mixing performance, the segregation index X_s is defined as follow [15]:

$$X_s = \frac{Y}{Y_{ST}} = \frac{V\left(C_{I_2} + C_{I_3^-}\right)}{n_{H^+,0}} \left(\frac{6C_{IO_3^-,0} + C_{H_2BO_3^-,0}}{3C_{IO_3^-,0}}\right) \quad (3)$$

Y represents the ratio of H^+ mole number consumed by reaction (ii) divided by the total H^+ mole number added. While Y_{ST} represents the value of Y when the micro mixing process is infinitely slow. V represents the total volume of the solution. n and C represent the mole number and mole concentration of the subscript

species, respectively [15]. As defined above, X_s should be 0 when there is a perfect mixing, while X_s should be 1 when there is complete segregation.

The unknown values, $C_{I_3^-}$ and C_{I_2}, can be calculated as follows [25]:

$$C_{I_3^-} = \frac{A}{K_\varepsilon} \tag{4}$$

$$\frac{5}{3}C_{I_2}^2 + \left(\frac{8}{3}C_{I_3^-} - C_{I^-,0}\right)C_{I_2} + \frac{C_{I_3^-}}{K_B} = 0 \tag{5}$$

In Eq. (4), A represents the absorbance of the solution under 353 nm-wavelength UV, K_ε represents the product of the molar extinction coefficient of triiodide ion and the wall thickness of cuvette, which is 26047 L/mol. In Eq. (5), K_B represents the equilibrium constant which relates to the temperature, and it is equal to 702 L/mol here under 298 K [25].

As shown in Fig. 1a, the experimental process is as follows: two advection pumps (2PB-10005) were used to inject the two initial solutions into the micromixer; then the UV spectrophotometer (Agilent Cary 60) was used to perform the absorbance measurement on the outflow solution, so as to obtain the concentration of triiodide produced in micromixer and calculate the value of X_s. The chemical agents used, including NaOH, KI, KIO_3, H_3BO_3, H_2SO_4, were all of the analytical purity. The initial solution A was made by diluting 98% H_2SO_4 solution. The initial solution B was made by mixing the solutions with certain concentrations of H_3BO_3, NaOH, KI, KIO_3 successively. The concentrations of species in the two initial solutions were as Tab. 3 [26].

Table 3: The concentration of species in the initial solutions

Initial solution	Species	Concentration (mol/L)
A	H^+	0.07
	IO_3^-	0.00233
B	$H_2BO_3^-$	0.0909
	I^-	0.01167

2.4 The Setup of CFD Simulation

As shown in Fig. 2b, the simulation models were founded by the boolean subtraction to the models shown in Fig. 1, and adding short asymmetric T-shape inlets. The simulation model without the designed inner unit was also founded, whose side length relied on the optimal gap width x of the designed models. The first converging zone is the place where the two initial solutions converge, while the main mixing zone is the main place for the mixing.

To simulate the flow field in the micromixer, the most widely used turbulent model: standard k-ε model was used. Moreover, the species transport equation was used to simulate the situation of the species diffusion. For reducing numerical diffusion, all the spatial discretizations were operated by using a higher-order discretization scheme Second Order Upwind. The velocity-inlet and outflow type were used at inlets and outlet, respectively. The volume flow rate of two inlets were set to 100 mL/min both in the chemical experiment and CFD simulation, because a relatively low volume flow rate of the inlet can magnify the difference of mixing efficiency among different micromixers [5]. The initial gauge pressure was set to 20000 Pa, which was close to the converged result and was beneficial to the converging process. Since the Reynolds number was relatively low due to the low volume flow rate, the enhanced wall treatment

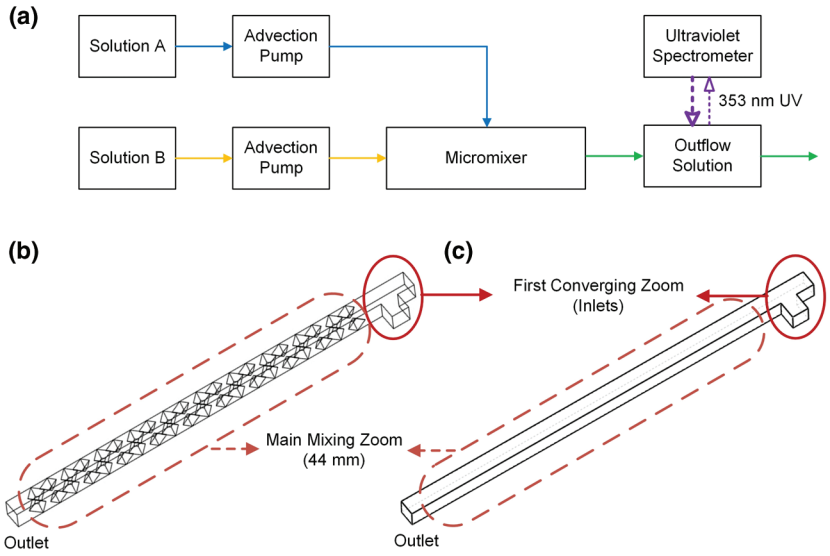

Figure 2: The process of the experiments and simulation models: (a) The process of the chemical experiment, (b) the simulation model with designed inner units, (c) the simulation model without designed inner unit

(EWT) was employed for higher accuracy [27]. The density and viscosity of both liquids entering into the two inlets were set to 997 kg/m^3 and 0.0008937 Pa·s, respectively. The mass diffusion coefficient of the mixture was set to 1×10^{-9} m^2/s [13]. The Ansys 17.0 was used, and the module was Fluent.

2.5 The Characterization of Mixing Efficiency in CFD Simulation

In order to characterize the mixing efficiency in CFD simulation that require less computing power, an index called intensity of mixing was put forward and has been confirmed by different studies [13,15,16,28,29]. This index is defined as Eq. (6).

In Eq. (6), I_M represents the intensity of mixing, σ^2 and σ^2_{max} represent the variance of mass fraction of the sample points inside the cross-section and the maximum value of σ^2 (which is 0.25 here) respectively. N represents the number of sample points inside the cross-section, c_i means the mass fraction of each sample point, and c_m (which is 0.5 here) means the optimal average mass fraction of the sample points inside the cross-section.

$$I_M = 1 - \sqrt{\frac{\sigma^2}{\sigma^2_{max}}}, \text{where } \sigma = \sqrt{\frac{1}{N}\sum_{i=1}^{N}(c_i - c_m)} \tag{6}$$

Since the simulation did not simulate the chemical experiment directly, I_M was not equal to X_s in the chemical experiment. However, they have the same logical connection to the mixing efficiency of micromixer. X_s is defined as the ratio of Y during the actual mixing to the Y_{ST} during complete segregation situation. Thus, a lower X_s shows a higher mixing efficiency. The ratio of σ^2/σ^2_{max} represents how the real mixing situation σ^2 is close to the complete segregation situation σ^2_{max} as well. To make I_M have the same trend to mixing efficiency, researchers subtracted the ratio of σ^2/σ^2_{max} from 1. Therefore, a higher I_M represents a higher mixing efficiency. If the trend between X_s and I_M is reversed, the simulation results could be predicted correctly.

3 Results

3.1 The Physical Models from SLM

As shown in Fig. 3a, each of the physical models had different exteriors to distinguish different models with variable gap widths. Since the wall thickness of the micromixer is thick enough, the external groove structures would not affect the formation of the internal unit body. Then, these models were welded with a standard tee coupling respectively, so that the two initial solutions could be injected into the channel together. Fig. 3b shows the inner units of this micromixer, whose features such as the gap and the front edge were formed as designed.

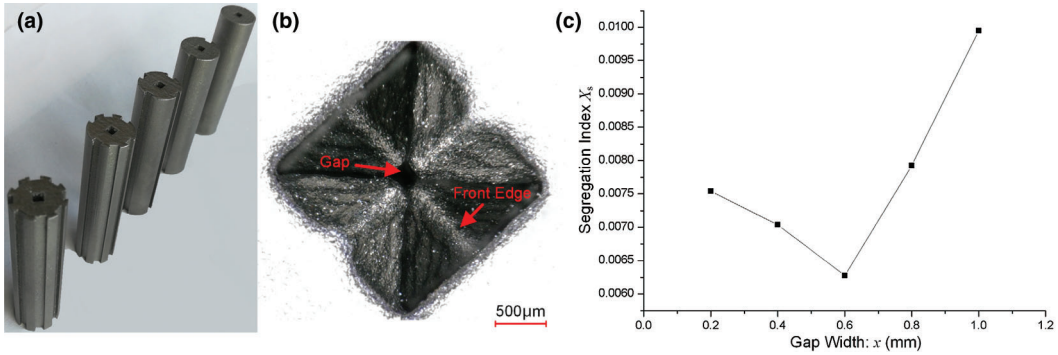

Figure 3: (a) the appearance of the physical models, (b) the appearance of the inner units, (c) Effect of gap width x on the segregation index X_s

3.2 The Results of the Chemical Experiment

The results of the chemical experiment are shown in Fig. 3c. With the increase of gap width as well as hydraulic diameter, the segregation index decreased at first and then increased sharply, which indicated that the mixing efficiency of the micromixer rose at first and then went down rapidly. This phenomenon deserves attention because the former researches have shown that the mixing efficiency of the conventional micromixer without any obstacle would monotonously decrease with the increase of hydraulic diameter [15] which was different from the situation here.

3.3 Mesh Independence Test and Mesh Selecting

Because CFD simulation is based on the discretization of digital models, it is necessary to ensure that the mesh is appropriate. Generally, when the scale of the mesh is at an interval where the simulation results hardly change along with the variety of mesh, the mesh may be appropriate. In this case, the dimensionless value of y^+ should also be considered to evaluate the mesh. It should be limited within 0~5 because of the use of EWT [27]. With the methods of global refinement and Mark/Adapt Cells, several meshes with different scales were created and applied to the simulation. In Fig. 4a, the curves of I_M of the simulations with x = 0.2 mm under the meshes with different scales are presented. It could be known that when the scale of mesh came to 3.16×10^6 elements, the curve of simulation result was very similar to the curve under the mesh with 1.35×10^6 elements, which meant the simulation results hardly changed along with the variety of mesh. Moreover, Fig. 4b shows the y^+ distribution of the simulation with x = 0.2 mm under the mesh with 3.16×10^6 elements, the value of y^+ varied within 0~5. Thus, the results under the mesh with 3.16×10^6 elements could represent the final results of the case with x = 0.2 mm. Following the same steps, the rest of mesh independence tests and mesh selecting processes were conducted.

3.4 Effect of Gap Width on I_M

Fig. 5a shows the effect of gap width on I_M, which was positively correlated with the mixing efficiency. The mixing efficiency predicted by CFD simulation had the same change tendency as the chemical

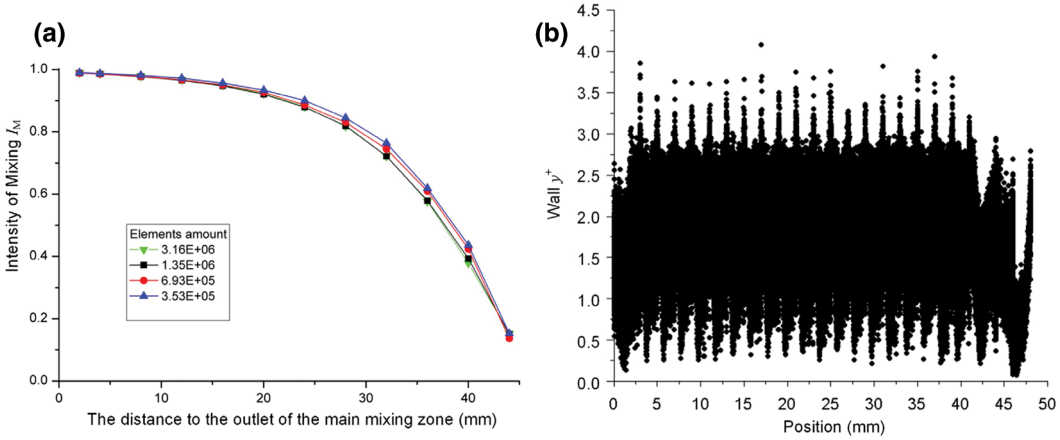

Figure 4: Mesh independence test and y^+ distribution: (a) Mesh independence test for the simulation with x = 0.2 mm; (b) The y^+ distribution of the simulation with x = 0.2 mm under the mesh with 3.16×10^6 elements

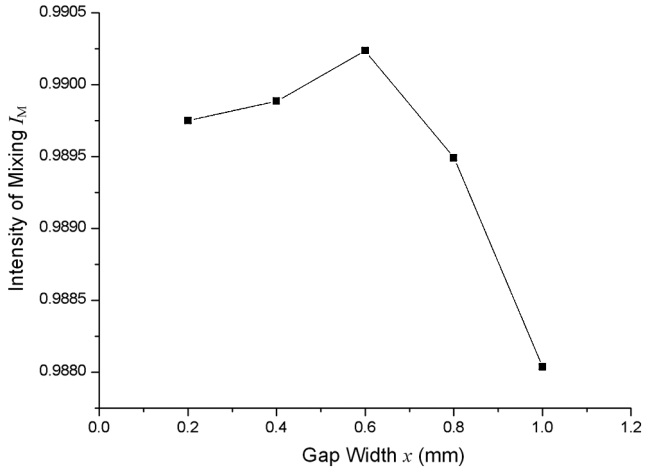

Figure 5: The effect of gap width x on the intensity of mixing I_M

experiment (increased first and then decreased sharply). Therefore, the results from the chemical experiment and CFD simulation shows that the gap width can influence the mixing efficiency.

In this paper, since the geometry of the inner units is determined by the gap width, it is worthy of investigating the relationship between gap width, geometry, and mixing efficiency. The following picture in Fig. 6a is the sketch showing the partitions of the geometry of the inner unit. The flow field of the

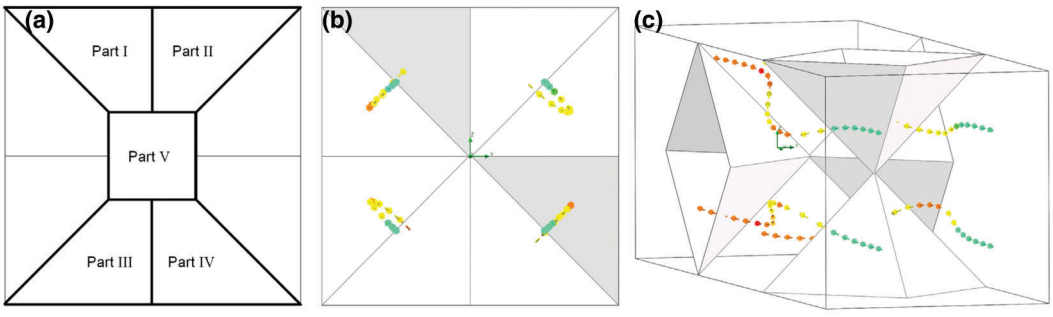

Figure 6: The definition of volume distribution of fluid: (a) when x is between 0 and 2; (b) and (c) when $x \to 0$

feature section can be divided into five parts, which represented five pieces of the fluid divided by front edges and gap. The variation of gap width would lead to different volume distribution of fluid in the five parts, and different volume distributions of fluid might cause different mixing efficiency. Here, the volume distribution of fluid was defined as the ratio of the area R_A between the area of part V and the area of part I since part I~IV were symmetrical. This definition could be expressed as Eq. (7):

$$R_{\mathrm{A}} = \frac{A_{\mathrm{partI}}}{A_{\mathrm{partV}}} = \frac{\frac{x+2}{2} \cdot \frac{2-x}{2} \cdot \frac{1}{2}}{x \cdot \left(2 - \frac{2-x}{2} \cdot 2\right)} = \frac{4-x^2}{8x^2}, (0 < x \leq 2) \tag{7}$$

Plugging 0.6 into x, which was the optimal gap width for the best mixing efficiency gained in this work. It can be solved that $R_{\mathrm{A}} \approx 1.26$, which approximately represented that the volume distribution of each part is uniform. This situation showed that uniform splits of fluid would be favourable to the improvement of mixing efficiency. It should also be noted that the variation tendencies of mixing efficiency in the processes of $x \to 0$ and $x \to 2$ was asymmetric. In the process of $x \to 2$, the mixing efficiency decreased faster than that in the process of $x \to 0$. Because, in the process of $x \to 0$, the mixing unit consists of two pairs of connected pyramids, as shown in Figs. 6b and 6c. The fluid tended to be divided into four pieces because the fluid in the same side (for example: left of right side) can be divided into two pieces with two opposite radial velocities, even though the two pieces is still connected. While in the process of $x \to 2$, fluid tended to be only one piece without being split. The more pieces of fluid were split out, the more pieces of fluid that collide, the easier it is for species to mix together.

3.5 The Advantages over Conventional Micromixer

Since the best gap width of the designed inner units was confirmed, the micromixer designed in this study can be compared with a conventional micromixer. The micromixer designed in this study was meliorated from the conventional micromixer which was a narrow channel without any inner unit (modeled as Fig. 2c) [15]. The feature size (hydraulic diameter) of the best micromixer in this research was 0.95 mm, corresponding to x = 0.6 mm. Therefore, set the side length of the conventional micromixer to 0.95 mm. According to Eq. (8), the volume flow rate of inlets should be adjusted to 47.5 mL/min with the change of the hydraulic diameter of inlets, so that the initial Reynolds number Re of inlets could be the same as the micromixer designed in this paper. In Eq. (8), ρ represents density, μ represents viscosity, and Q_v represents the volume flow rate of the cross section.

$$Re = \frac{\rho v_{\mathrm{avr}} d}{\mu} = \frac{\rho \cdot \frac{Q_v}{d^2} \cdot d}{\mu} = \frac{\rho}{\mu} \cdot \frac{Q_v}{d} \tag{8}$$

As the most concerned aspect, the mixing efficiency was discussed firstly. In Fig. 7, the curve of channel A represents the mixing efficiency of the micromixer with a gap designed of 0.6 mm, and the other curve represents the mixing efficiency of the conventional micromixer without any inner unit. It could be inferred that at the beginning of the main mixing zone, channel B has better mixing efficiency than channel A because it has a transition zone. In the transition zone of channel A, the fluid regime was laminar as in the channel B, because there were no inner unit at transition zone and the critical Reynolds number of the square section is 2070 [30], which was much higher than 930 in this case. In the laminar regime, the type of diffusion is molecular diffusion, which depends on concentration difference and hydraulic diameter. Since the hydraulic diameter of channel B was 0.95 mm, and the hydraulic diameter of the transition zone of channel A was 2 mm, the molecular diffusion in channel B was faster than the transition zone of channel A.

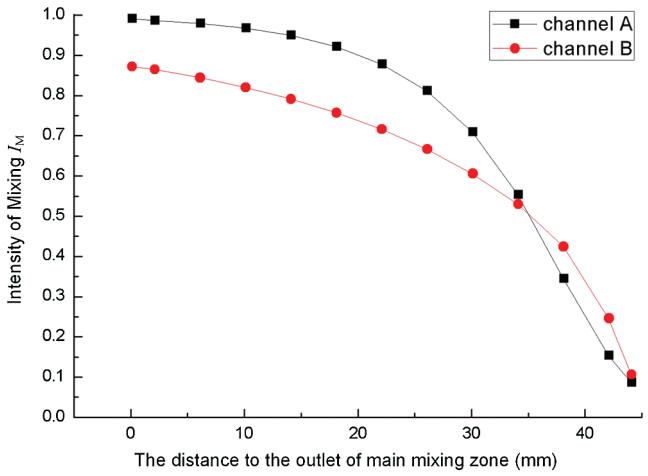

Figure 7: The comparison in mixing efficiency ($Re_{0,\,A} = Re_{0,\,B} = 930$) channel A: the novel micromixer with a gap width of 0.6 mm; channel B: the tradition micromixer without obstacle

After the transition zone, fluid would flow through the inner units, which disturbed the flow, reduced the critical Reynolds number and resulted in turbulence. In the turbulence regime, the main type of diffusion turned to convection diffusion which would take charge of the diffusion process due to a much higher effective diffusion coefficient [27]. At the third sampling point in Fig. 7, the fluid has flowed through the first inner unit, and the disparity between these two curves has begun to decrease. After the fluid flowed through the fourth sampling point of the second internal unit, the mixing efficiency of channel A started to be better than that of channel B, and this situation continued to the end of the channel.

As shown in Fig. 8, the inner units designed in this research caused more negative pressure zones than the conventional one, which indicated that there was more reverse flow happening in the channel A. Reverse flow is one of the origins to form swirls. Generally, more reverse flow regions bring more swirls, and the swirls can pull the nearby fluid together, which shortens the diffusion distance of species and improve mixing efficiency.

From Fig. 7, it could be inferred that the mixing efficiency of channel A at the section which was 22 mm far from the outlet was nearly equal to that of channel B at the outlet. Also, it could be known from Fig. 8 that

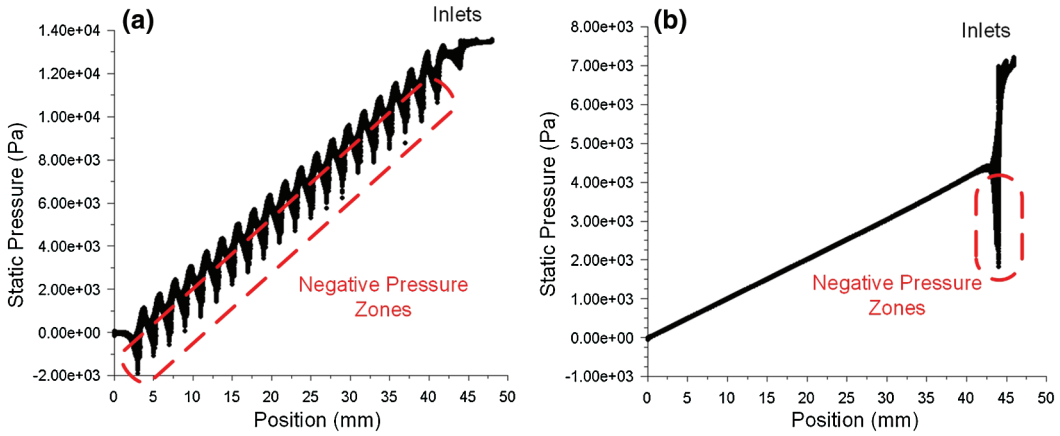

Figure 8: The comparison in pressure drop: (a) the pressure plot of channel A, (b) the pressure plot of channel B, $Re_{0,\,A} = Re_{0,\,B} = 930$

the pressure drop of channel A from inlets to the section above was about 6500 Pa, and the pressure drop of channel B from inlets to outlet was about 7250 Pa. Therefore, the micromixer designed in this research not only improved the mixing efficiency, but also reduced the pressure drop of 10.34%, which means lower power requirements and energy saving.

In Fig. 9, the flow fields were presented by streamlines. When two pieces of fluid entered the inlets, they came to the first converging zone and collided for the first time. This process happened in both channel A and channel B, caused the first swirl. However, when the fluid came to the main mixing zone, the situation started to be different. In channel A, the fluid was led by the inner units. They collided again and again, forming swirls, which confirmed the conclusions of Fig. 8. The swirls in channel A also constantly disturbed the flow, resulting in the flow maintaining turbulence in the main mixing zone, which enhanced convection diffusion and mixing. On the contrast, there was no swirl produced in the main mixing zone of channel B. Thus, the flow regime came back to laminar, which went against the improvement of mixing efficiency.

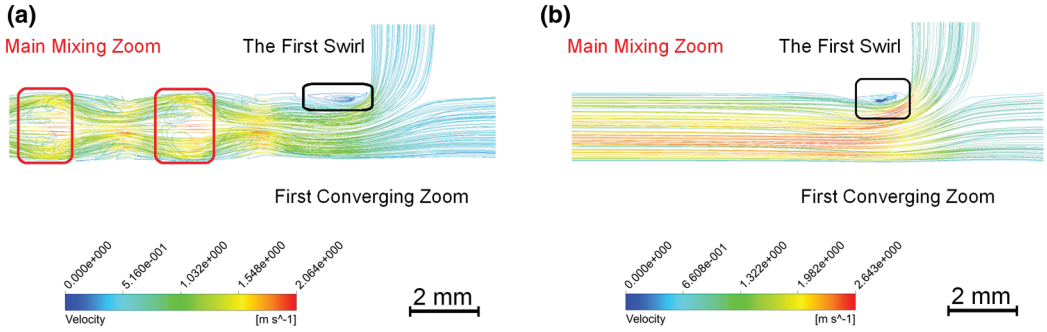

Figure 9: The comparison in flow field: (a) the streamlines of channel A, (b) the streamlines of channel B, $Re_{0,\,A} = Re_{0,\,B} = 930$

4 Discussions

4.1 The Mixing Behaviour in the Novel Micromixer

As is stated above, the reason why the novel micromixer in this paper has a better mixing efficiency than the conventional one is the introduction of more fluid collision and swirls. In this section, more details will be presented to show the mixing behaviour in the novel micromixer. In the following pictures, some cross-sections of the flow field are picked out, and the pressure contours and velocity vector diagrams of them are presented.

From the view of force and motion, Fig. 11 shows how the inner units act on fluid. The locations of selected a~b cross-sections are shown as Fig. 11A. For the flow field, the influence of gravity is negligible because of the small width and length of the channel. Thus, the flow field is mainly driven by the pressure difference which determines the direction of acceleration and how the fluid moves eventually.

It can be found that at the beginning, the high-pressure zones appear at the places where the fluid hits the front edges of obstacles because the obstacles bring anti-force to the fluid while the central region does not. Therefore, the acceleration vectors point from the front edges to the central zone and so do the velocity vectors as the vector diagrams shown in Figs. 11a2 and 11b2. In the zone before the middle cross-section of obstacles, the mixing behaviour is mainly collision.

As the colliding progresses, the high-pressure zones appear in the converging zones of the central region due to the reaction force generated by colliding. Meanwhile, the obstacles no longer obstruct the fluid after the fluid has flowed through the middle cross-section of the obstacle. Therefore, there are some low-pressure zones close to the back slopes. Then, the acceleration vectors point from the central region to the

surrounding. The acceleration vectors are opposite to the velocity vectors, resulting that the torque appears because not all acceleration vectors are on the same lines as velocity vectors. The torque causes swirls. Thus, in the zone following the middle cross-section of obstacles, the mixing behaviour is the development of swirls and the collisions between different swirl boundaries.

As mentioned above, there are two mixing patterns. One is the collision and the other is the swirl. Fig. 10 shows how these two mixing patterns influence the mixing process. In hydrodynamics theory system, the continuous fluid can be divided into plenty of micro masses with different physical or chemical states. The collision is defined as the colliding between two fluid micro masses. When two micro masses collide, the species contained in the micro masses will cross the boundary between two micro masses, resulting in the mixing of two species. Also, the larger micro mass will be divided into some smaller micro masses by collision. With a smaller volume, the micro masses can obtain a larger specific area that can increase the contact area between the micro masses and the environment, which is conducive to the molecular diffusion caused by the difference in the concentration.

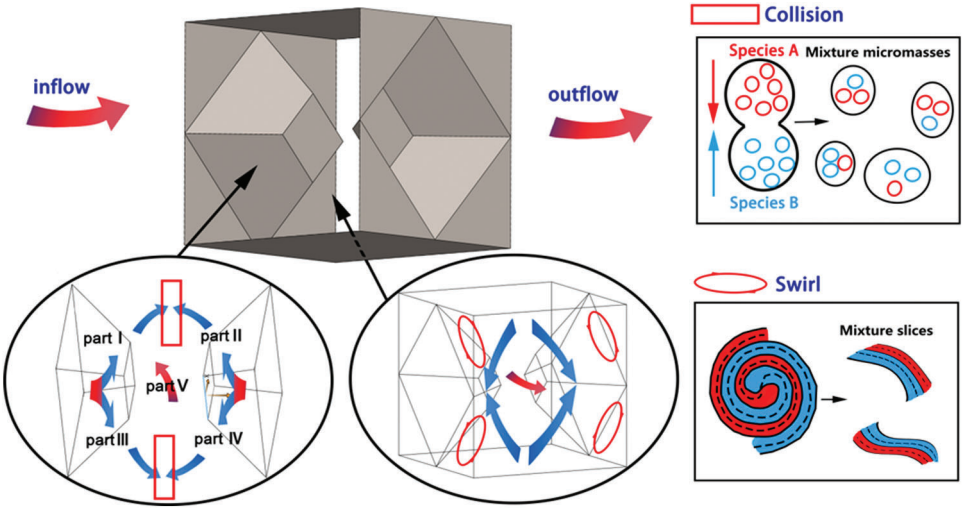

Figure 10: The sketch of the mixing process

In swirls, the fluid orbits around a low-pressure point and moves along a helical line. Thus, the fluid micro masses do not hit each other directly. The mixing mainly occurs when the molecules diffuse through the boundary between two micro masses, and the mixing efficiency mainly depends on the size of the contact area. Owing that fluid is not a rigid body, the shape of fluid can be changed easily by force. Thus, when fluid orbits in swirls, the fluid micro masses are drawn into thin and long slices by the normal and tangential accelerations caused by pressure difference and viscous force. The slice form of fluid micro masses can offer a much larger contact area between two micro masses, resulting in stronger molecule diffusion and better mixing efficiency.

Figs. 11c–11f presents the development process of swirls, including its appearing, growing, dissipating and disappearing. At the same time, the number of swirls, the size of the swirls, the energy contained in the swirls and other characteristics of the swirls change with the development of the swirls. The text above has only explained the mixing process in one swirl. However, how the geometry of the inner unit influences the development of the swirl and what the mixing process is like at each stage of swirl development still needs further research.

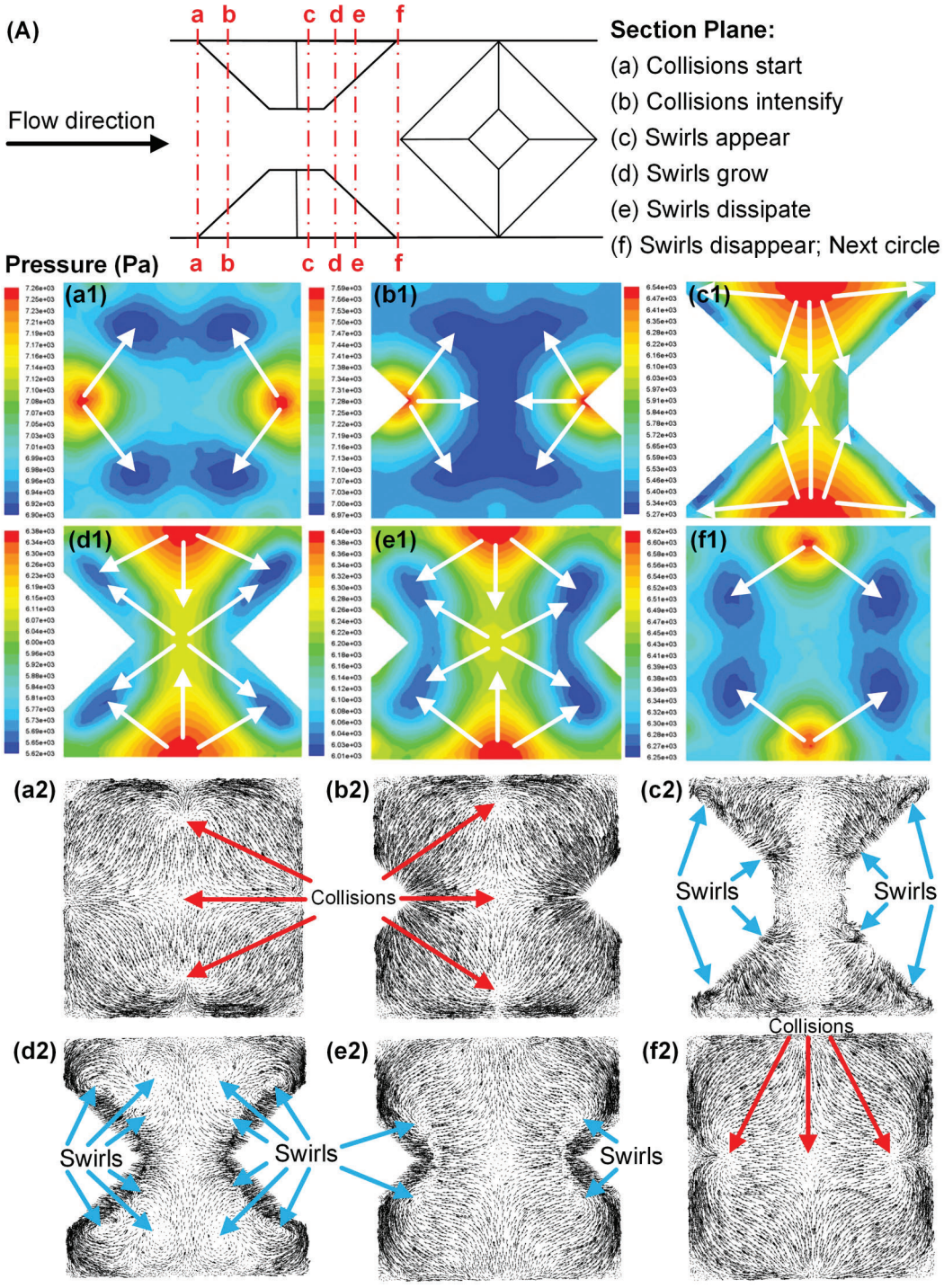

Figure 11: The mixing process of the novel micromixer: (A) the locations of the selected cross-sections, (a1~f1) the pressure contours and (a2~f2) the velocity vector diagrams of each selected cross-section, which are from the simulation with x = 0.6 mm

4.2 The Application Scheme

The production of the complex geometry of inner units inside the micromixer requires the help of AM. Because the microreactors designed in this research are small in size, there is no need to use a large AM equipment to produce the micromixer, which can save equipment and space, thereby saving money. Also, the small size allows a compact placement on a substrate plate, which is benefit to the productivity. To reach a balance between material cost and pressure resistance, the wall thickness of the micromixers can often be requested to change according to the working conditions, which demands high flexibility of the manufacturing technology. With AM, it is simple to achieve this flexibility by just adjusting the CAD models.

In this paper, the chemical experiment and CFD simulation were conducted based on the mixture liquid whose density and viscosity were very close to the water, which has a very low viscosity. However, the viscosity of liquids such as methylbenzene and other organic solvents used in actual production is often several orders of magnitude higher than that of water, while the density of these organic solvents is usually the same order of magnitude as that of water.

As a result, it is much more difficult for the liquid used in actual production to enter a turbulent flow regime than the liquid used in this paper. This difference will result in a lower mixing efficiency in actual production than in this research. The solution to this problem is to extend the length of micromixers properly. Thanks to the flexibility of AM, the extending in three dimensions is convenient. As shown in Fig. 12, in addition to straight tubes, manufacturing tests of different shapes of micromixers, such as "U-shaped" or "S-shaped", have been performed.

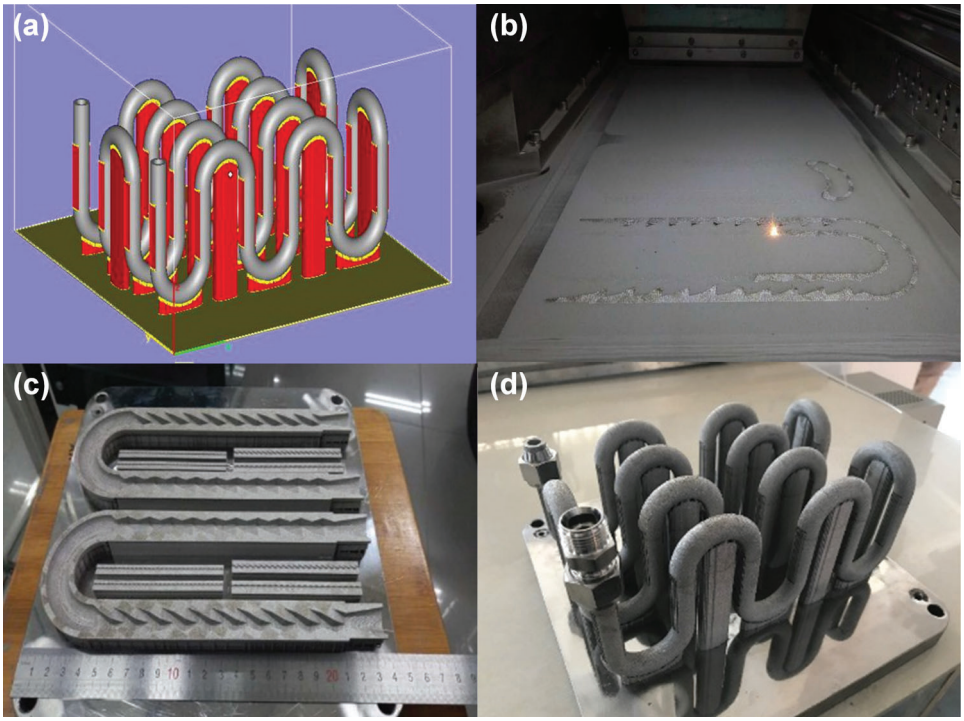

Figure 12: The design and additive manufacturing to extend the length of micromixer: (a) the design of CAD model; (b) additive manufacturing; (c) observation of the micromixer internal structure by Wire Electrical Discharge Machining (WEDM); (d) welding joints

5 Conclusions

In this work, a novel micromixer was developed. The mixing efficiency and pressure drop of it were investigated. With the designed inner geometry and the chosen parameters (hole width: 2 mm, channel length: 44 mm, gap width: 0.6 mm, line-face angle: 45°), high mixing efficiency with I_M up to 0.9902 can be achieved (very close to the complete mixing with I_M equal to 1). The pressure drop of the novel micromixer was relatively low (10.34% lower than the conventional ones), which showed a relatively low energy request.

Besides, the mechanism to improve the mixing efficiency was investigated as well. The results showed that by leading fluid separation and collision, the species of one fluid micro mass could enter another micro mass more easily, thereby promoting the exchange of substances inside the flow field. To obtain the best separation and collision process, the inner units should be designed to evenly disperse the fluid. Furthermore, the collisions of fluid would cause a pressure difference against the original flow direction, which produced the swirls that could draw the fluid into thin and long slices, increasing the size of contact area, strengthening the molecule diffusion, and improving mixing efficiency.

At last, the application scheme of the micromixer was discussed briefly. Firstly, it can be sure that AM is suitable for the reforming of micromixer. With AM, the production of this micro-mixer has high productivity and manufacturing flexibility. Secondly, considering the physical properties of the liquid used in real production, the length of the micromixer should be able to be extended properly. And could be enlarged in three dimensions.

Funding Statement: This project was supported by the National Natural Science Foundation of China (51775196), Guangdong Province Science and Technology Project (2017B090912003, 2017B090911014), High-level Personnel Special Support Plan of Guangdong Province (2016TQ03X289), Guangzhou Star of Pearl River Talent Project (201710010064), the Fundamental Research Funds for the Central Universities (Project Nos. 2018ZD30, 2019MS060), Guangzhou Science and Technology Project (201704030097). The authors would like to thank for these financial supports.

Conflicts of Interest: The authors declare that they have no conflicts of interest to report regarding the present study.

References

1. Kockmann, N., Kiefer, T., Engler, M., Woias, P. (2006). Convective mixing and chemical reactions in microchannels with high flow rates. *Sensors and Actuators B: Chemical, 117(2),* 495–508. DOI 10.1016/j.snb.2006.01.004.
2. Hanks, M. L., Toor, H. L. (1995). Relative importance of macro- and micromixing in turbulent, reacting jets. *Industrial & Engineering Chemistry Research, 34(10),* 3252–3256. DOI 10.1021/ie00037a011.
3. Kunowa, K., Schmidt-Lehr, S., Pauer, W., Moritz, H. U., Schwede, C. (2007). Characterization of mixing efficiency in polymerization reactors using competitive-parallel reactions. *Macromolecular Symposia, 259(1),* 32–41. DOI 10.1002/masy.200751305.
4. Meyer, T. (2002). Scale-up of polymerization processes. *Current Opinion in Drug Discovery & Development, 5(6),* 960–965.
5. Wang, L. (2016). *Design and application of microreactor*. Beijing: Chemical Industry Press, China.
6. Mansur, E. A., Ye, M. X., Wang, Y. D., Dai, Y. Y. (2008). A state-of-the-art review of mixing in microfluidic mixers. *Chinese Journal of Chemical Engineering, 16(4),* 503–516. DOI 10.1016/S1004-9541(08)60114-7.
7. Richmond, C. J., Miras, H. N., De la Oliva, A. R., Zang, H. Y., Sans, V. et al. (2012). A flow-system array for the discovery and scale up of inorganic clusters. *Nature Chemistry, 4(12),* 1037–1043. DOI 10.1038/nchem.1489.

8. Fan, X. L., Sans, V., Yaseneva, P., Plaza, D. D., Williams, J. et al. (2012). Facile stoichiometric reductions in flow: an example of artemisinin. *Organic Process Research & Development, 16(5),* 1039–1042. DOI 10.1021/op200373m.
9. Sebastian, V., Smith, C. D., Jensen, K. F. (2016). Shape-controlled continuous synthesis of metal nanostructures. *Nanoscale, 8(14),* 7534–7543. DOI 10.1039/C5NR08531D.
10. Briggs, M. E., Slater, A. G., Lunt, N., Jiang, S., Little, M. A. et al. (2015). Dynamic flow synthesis of porous organic cages. *Chemical Communications, 51(98),* 17390–17393. DOI 10.1039/C5CC07447A.
11. Hessel, V., Löwe, H., Schönfeld, F. (2005). Micromixers—a review on passive and active mixing principles. *Chemical Engineering Science, 60(8–9),* 2479–2501. DOI 10.1016/j.ces.2004.11.033.
12. Su, Y. H., Kuijpers, K., Hessel, V., Noël, T. (2016). A convenient numbering-up strategy for the scale-up of gas-liquid photoredox catalysis in flow. *Reaction Chemistry & Engineering, 1(1),* 73–81. DOI 10.1039/C5RE00021A.
13. Engler, M., Kockmann, N., Kiefer, T., Woias, P. (2004). Numerical and experimental investigations on liquid mixing in static micromixers. *Chemical Engineering Journal, 101(1–3),* 315–322. DOI 10.1016/j.cej.2003.10.017.
14. Bettermann, S., Kandelhard, F., Moritz, H. U., Pauer, W. (2019). Digital and lean development method for 3D-printed reactors based on CAD modeling and CFD simulation. *Chemical Engineering Research and Design, 152,* 71–84. DOI 10.1016/j.cherd.2019.09.024.
15. Liu, Z. D., Lu, Y. C., Wang, J. W., Luo, G. S. (2012). Mixing characterization and scaling-up analysis of asymmetrical T-shaped micromixer: experiment and CFD simulation. *Chemical Engineering Journal, 181,* 597–606.
16. Ansari, M. A., Kim, K. Y., Anwar, K., Kim, S. M. (2010). A novel passive micromixer based on unbalanced splits and collisions of fluid streams. *Journal of Micromechanics and Microengineering, 20(5),* 055007. DOI 10.1088/0960-1317/20/5/055007.
17. Sing, S. L., Yeong, W. Y., Wiria, F. E., Tay, B. Y., Zhao, Z. Q. et al. (2017). Direct selective laser sintering and melting of ceramics: a review. *Rapid Prototyping Journal, 23(3),* 611–623. DOI 10.1108/RPJ-11-2015-0178.
18. Gu, D. D., Meiners, W., Wissenbach, K., Poprawe, R. (2012). Laser additive manufacturing of metallic components: materials, processes and mechanisms. *International Materials Reviews, 57(3),* 133–164. DOI 10.1179/1743280411Y.0000000014.
19. Okafor, O., Weilhard, A., Fernandes, J. A., Karjalainen, E., Goodridge, R. et al. (2017). Advanced reactor engineering with 3D printing for the continuous-flow synthesis of silver nanoparticles. *Reaction Chemistry & Engineering, 2(2),* 129–136. DOI 10.1039/C6RE00210B.
20. Guo, M. Z., Hu, X. J., Yang, F., Jiao, S., Wang, Y. J. et al. (2019). Mixing performance and application of a three-dimensional serpentine microchannel reactor with a periodic vortex-inducing structure. *Industrial & Engineering Chemistry Research, 58(29),* 13357–13365. DOI 10.1021/acs.iecr.9b01573.
21. Frazier, W. E. (2014). Metal additive manufacturing: a review. *Journal of Materials Engineering and Performance, 23(6),* 1917–1928. DOI 10.1007/s11665-014-0958-z.
22. Guichardon, P., Falk, L. (2000). Characterisation of micromixing efficiency by the iodide-iodate reaction system. Part I: experimental procedure. *Chemical Engineering Science, 55(19),* 4233–4243. DOI 10.1016/S0009-2509(00)00068-3.
23. Kölbl, A., Kraut, M., Schubert, K. (2008). The iodide iodate method to characterize microstructured mixing devices. *AIChE Journal, 54(3),* 639–645. DOI 10.1002/aic.11408.
24. Baccar, N., Kieffer, R., Charcosset, C. (2009). Characterization of mixing in a hollow fiber membrane contactor by the iodide-iodate method: numerical simulations and experiments. *Chemical Engineering Journal, 148(2–3),* 517–524. DOI 10.1016/j.cej.2008.12.020.
25. Commenge, J. M., Falk, L. (2011). Villermaux–Dushman protocol for experimental characterization of micromixers. *Chemical Engineering and Processing: Process Intensification, 50(10),* 979–990. DOI 10.1016/j.cep.2011.06.006.
26. Fournier, M. C., Falk, L., Villermaux, J. (1996). A new parallel competing reaction system for assessing micromixing efficiency-experimental approach. *Chemical Engineering Science, 51(22),* 5053–5064. DOI 10.1016/0009-2509(96)00270-9.

27. ANSYS, Inc. (2016). ANSYS Fluent User's Guide, Release 17.0.
28. Lu, L. H., Ryu, K. S., Liu, C. (2002). A magnetic microstirrer and array for microfluidic mixing. *Journal of Microelectromechanical Systems, 11(5),* 462–469. DOI 10.1109/JMEMS.2002.802899.
29. Chung, C. K., Shih, T. R. (2007). A rhombic micromixer with asymmetrical flow for enhancing mixing. *Journal of Micromechanics and Microengineering, 17(12),* 2495–2504. DOI 10.1088/0960-1317/17/12/016.
30. Zhang, G., Wu, J. (2012). *Fluid dynamics*. Beijing: China Machine Press, China.